

pubs.acs.org/Macromolecules Article

# All-Polylactones Nano-Objects Prepared by a One-Pot Ring-Opening Polymerization-Induced Self-Assembly Process

Ding Shen, Boyang Shi, Peng Zhou, Di Li, Wenya Zhu, and Guowei Wang\*



**Cite This:** *Macromolecules* 2024, 57, 8970–8982



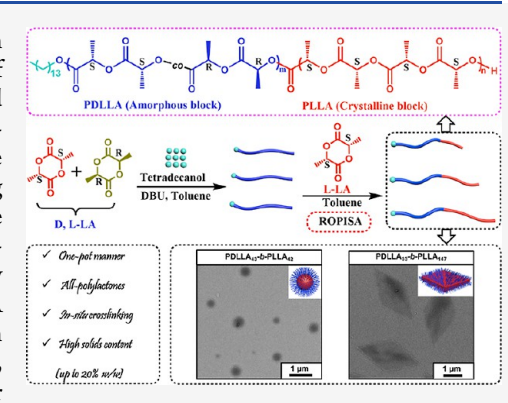
**ACCESS** I

III Metrics & More

Article Recommendations

s Supporting Information

**ABSTRACT:** Ring-opening polymerization (ROP) has been acknowledged as an efficient approach to biodegradable polylactones. Herein, by a sequential ROP of D<sub>J</sub>L-lactic acid (D<sub>J</sub>L-LA) and L-lactic acid (L-LA) monomers in toluene, we reported a ROP-induced self-assembly (ROPISA) process. The poly(D<sub>J</sub>L-lactic acid)-b-poly(L-lactic acid) (PDLLA-b-PLLA)-based all-polylactones nano-objects were prepared in a one-pot manner. The crystalline PLLA served as a core-forming block, and amorphous PDLLA acted as a stabilizer block. The morphologies of the generated nano-objects included spheres and platelets by varying the polymerization parameters. Uniquely, the ROPISA was synergistically driven by crystallization and solubility of the PLLA core. The versatility of the ROPISA process was also demonstrated by the successful preparation of nano-objects with poly(ε-caprolactone) (PCL) or poly(δ-valerolactone) (PVL) as the stabilizer block, and PLLA as the core-forming block. Based on the living and controlled character



of ROPISA, in the final polymerization, the living species in the PLLA core could be *in situ* cross-linked by 4.4'-bioxepanyl-7.7'-dione (BOD) and the nano-objects could be stabilized. The melting temperature  $(T_{\rm m})$  of the polylactone blocks in the core or shell region was independent and unaffected. Comparing with the unstabilized nano-objects, the thermal stability of stabilized nano-objects can be significantly enhanced.

# ■ INTRODUCTION

The polylactones [e.g., poly( $\varepsilon$ -caprolactone) (PCL), poly( $\delta$ -valerolactone) (PVL), poly(glycolic acid) (PGA), and poly-(lactide) (PLA)], as environmentally friendly alternatives, have gained increasing attention owing to their unique biocompatibility and biodegradability. The polylactones with predictable molecular weight (MW), narrow MW distribution ( $M_{\rm w}/M_{\rm n}$ ), and high end group fidelity have given rise to a broad range of practical applications, including packaging, agriculture, and especially biomedical fields, such as drug delivery, and cancer immunotherapy, tissue scaffold, and so on.

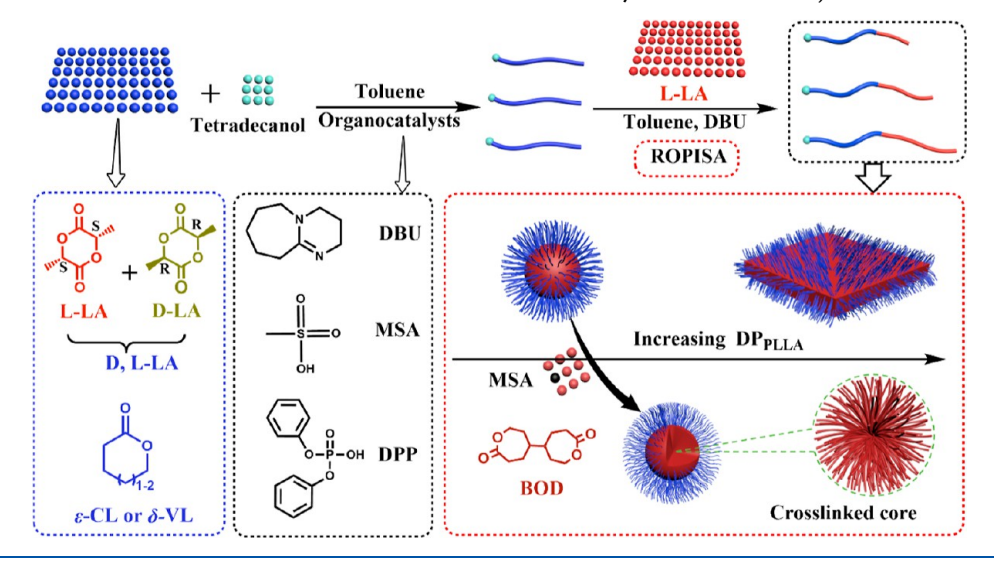
PLA, owing to its excellent properties as well as the "green" synthetic route, has been well studied and extensively applied. For instance, more than 15 PLA-based micro/ nanoparticle products had been approved and marketed. <sup>14</sup> In most practical applications, it was a highly desirable approach to introduce PLA as a block in copolymers, which can be further constructed as self-assembled nano-objects with controlled morphologies and functions. For example, Han et al. 15 had investigated the self-assembly of poly(L-lactic acid)-bpolystyrene (PLLA-b-PS) diblock copolymers in selective solvents of the carbon disulfide (CS<sub>2</sub>)/tetrahydrofuran (THF) mixture and the lamellar nano-objects were captured. O'Reilly et al. 16 had prepared spherical and cylindrical nanoobjects by direct dissolution of poly(D,L-lactide)-b-poly(acrylic acid) (PDLLA-b-PAA) or poly(L-lactide)-b-poly(acrylic acid) (PLLA-b-PAA) block copolymers in water. Interestingly, they observed the formation of spherical nano-objects with stereocomplex cores by self-assembly of a mixture of PLLAb-PAA and PDLA-b-PAA in water. To Subsequently, they further studied the self-assembly of poly(4-acryloyl morpholine)-b-poly(L-lactide) (P4AM-b-PLLA), methoxy polyethylene glycol-b-poly(L-lactide)(mPEG-b-PLLA), and poly(N,Ndimethylacrylamide)-b-poly(L-lactide) (PDMA-b-PLLA) block copolymers<sup>18</sup> and explored the nano-objects as antibacterial agents, emulsifiers, adhesives, etc. 19-21 Manners et al. 22 had prepared a series of well-controlled and unprecedented hierarchical 2D structures using poly(4-vinylpyridine)-b-poly-(L-lactide) (P4VP-b-PLLA) via the seeded growth route. Chen et al.<sup>23,24</sup> prepared a series of sphere, fiber, and platelet nanoobjects using PLLA as the core and glycopolymers as the shell. They expected that the glyco-functionalized nano-objects with different morphologies and dimensions would open a new avenue for immunological therapeutics. However, based on the above examples of self-assembly systems, the nano-objects

Received: June 10, 2024
Revised: August 25, 2024
Accepted: September 4, 2024
Published: September 19, 2024





Scheme 1. Schematic of the ROPISA Process and Stabilization of All-Polylatones Nano-Objects



were mostly featured with complex operation steps and relatively low concentrations (<1.0% w/w).<sup>2.5</sup>

The polymerization-induced self-assembly (PISA) has been demonstrated for constructing nano-objects with simple operation and relatively high solids content (up to 50% w/ w), 26-30 which addressed the above-mentioned issues and further facilitated the practical applications.<sup>31–34</sup> However, in most conventional PISA systems, the core-forming block was noncrystallizable. Alternatively, when a crystallizable coreforming block (such as the polylactones of PLLA, PCL, PVL, etc.) is introduced into a PISA system, crystallization will become the primary driving force. This will consequently lead to the formation of nano-objects with distinct morphologies from those obtained using the conventional PISA system. 35,36 The crystallizable polylactones were generally synthesized by the ring-opening polymerization (ROP) mechanism. 37-39 Correspondingly, the ROP-induced self-assembly (ROPISA) of lactones should be an optimized route for nano-objects with crystallizable core-forming block.<sup>40</sup> For instance, Patterson et al. 41,42 performed the ROPISA process of the L-LA monomer using mPEG-OH as the macroinitiator. Du et al.  $^{43}$  and Bonduelle et al. 44,45 realized the ROPISA process of the Ncarboxyanhydride (NCA) monomer using mPEG-NH<sub>2</sub> as the macroinitiator. Alternatively, Yang et al. 46 and Manners et al. 47 reported the ROPISA process of fluorene trimethylene carbonate (FTMC) and salicylic acid o-carboxyanhydride (SAOCA) monomers using mPEG-OH as the macroinitiator. Without exception, mPEG was mostly employed as the macroinitiator/stabilizer, and the ROPISA was dominantly realized via a two-stage process. Aiming to develop the ROPISA technique, in our previous work, 48 we performed a ROPISA process using hydroxyl-terminated polyisobutylene (PIB-OH) as macroinitiator and PCL or PVL as core-forming block. Although the available macroinitiator/stabilizer and core-forming blocks were enriched, a two-stage process was also required. Given the increasing requirements on polylactone-based nano-objects, further development on the ROPISA technique is still urgent.

Recently, a tentative experiment showed that <sub>D,L</sub>-lactic acid (D,L-LA) and L-lactic acid(L-LA) monomers can be polymerized using the same catalyst of 1,8-diazabicyclo[5.4.0]-undec-7-ene (DBU). However, the resulting PDLLA and

PLLA have distinct solubility in toluene. This phenomenon inspired us to target the all-polylactide-based nano-objects by a one-pot ROPISA process, which is hoped to simplify the synthetic route to nano-objects and correspondingly facilitate their applications. Herein, all-polylactides nano-objects with amorphous PDLLA as the stabilizer/macroinitiator block and crystallizable PLLA as the core-forming block were realized by the sequential ROPISA process using 1-tetradecanol, toluene, DBU, D,L-LA, and L-LA as the initiator, solvent, catalyst, and monomers, respectively (Scheme 1). The factors of the degree of polymerization (DP) of PDLLA (DPPDLLA) or PLLA (DP<sub>PLLA</sub>), solids content and solvents on the morphological evolution were systematically monitored, and the morphologies of spheres and diamond-shaped platelets were captured from the PDLLA-b-PLLA-based ROPISA system. Furthermore, a similar strategy can also be performed for poly( $\varepsilon$ caprolactone)-b-poly(L-lactic acid) (PCL-b-PLLA) or poly( $\delta$ valerolactone)-b-poly(L-lactic acid) (PVL-b-PLLA)-based allpolylatones nano-objects, demonstrating wide applicability of the ROPISA process. The nano-objects can be stabilized by in situ cross-linking of living species using a degradable crosslinker of 4,4'-bioxepanyl-7,7'-dione (BOD) in the final polymerization stage. The thermal properties of all-polylatone nano-objects were also performed and compared.

#### ■ RESULTS AND DISCUSSION

Practicability of ROPISA Using Amorphous PDLLA as the Stabilizer Block and Crystallizable PLLA as the Core-Forming Block. Employing DBU, toluene, and 1-tetradecanol as the catalyst, solvent, and initiator, respectively, the PDLLA stabilizer/macroinitiator block was synthesized by ROP of the D,L-LA monomer in the first polymerization stage. Subsequently, in the second polymerization stage, the L-LA monomer was added, and the PDLLA-b-PLLA diblock copolymer was generated. As the toluene was a good solvent for the PDLLA block and a simultaneously poor solvent for the PLLA block, the generated PDLLA-b-PLLA favored to aggregate with the gradual chain extension of the PLLA block, and the ROPISA process was thus realized.

Using the synthesis of PDLLA<sub>18</sub>-b-PLLA<sub>38</sub> as an example, the ROPISA process was realized by sequential addition of D, L-LA, and L-LA monomers with a solid content of 10% w/w at

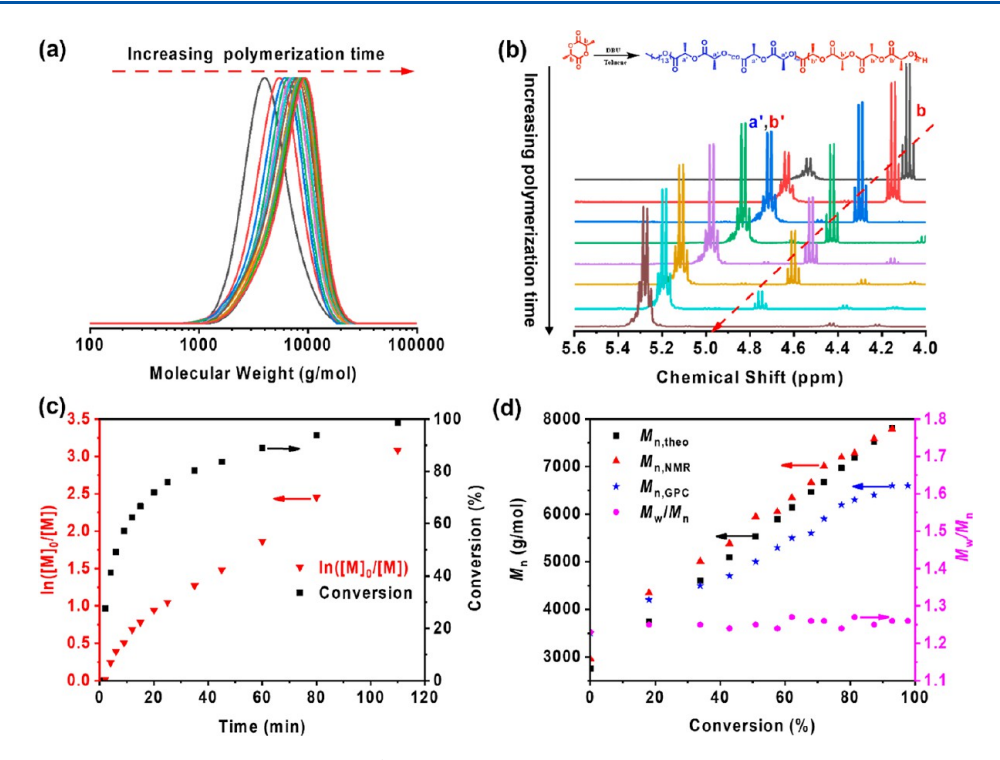


Figure 1. Polymerization kinetics for the ROPISA process (targeted at PDLLA<sub>18</sub>-b-PLLA<sub>38</sub> with a solid content of 10% w/w at the temperature of 20 °C and stirring rate of 300 rpm): (a) GPC curves of PDLLA and PDLLA-b-PLLA diblock copolymers at different polymerization times, (b)  $^{1}$ H NMR spectra of crude product at different polymerization times (in CDCl<sub>3</sub>), (c) plots of monomer conversion and ln([M]<sub>0</sub>/[M]) versus time, and (d) plots of  $M_{\rm n,heo}$ ,  $M_{\rm n,NMR}$ ,  $M_{\rm n,GPC}$ , and  $M_{\rm w}/M_{\rm n}$  versus monomer conversion.

Table 1. Formulation, Characterization, and Morphologies of Nano-Objects Obtained in the ROPISA Process<sup>a</sup>

entry	samples <sup>b</sup>	actual $\mathrm{DP}_{\mathrm{PDLLA}}/\mathrm{DP}_{\mathrm{PLLA}}$	the first polymerization stage			the second polymerization stage			morphologies <sup>d</sup>
			$M_{ m n,NMR}^{b} ({ m g/mol})$	$M_{n,GPC}^{c}$ (g/mol)	$M_{ m w}/{M_{ m n}}^c$	$\frac{M_{ m n,NMR}}{({ m g/mol})}^{b}$	$M_{n,GPC}^{c}$ (g/mol)	$M_{\rm w}/{M_{\rm n}}^c$	
1	PDLLA <sub>35</sub> -b-PLLA <sub>10</sub>	3.50	5000	5400	1.17	6400	6600	1.25	irregular morphology
2	$PDLLA_{34}$ - $b$ - $PLLA_{18}$	1.89	4900	5300	1.18	7600	7600	1.30	sphere
3	$PDLLA_{43}$ - $b$ - $PLLA_{42}$	1.02	6100	5700	1.18	12,200	11,000	1.24	sphere
4	PDLLA <sub>34</sub> -b-PLLA <sub>58</sub>	0.58	4900	5200	1.24	13,200	9200	1.32	sphere and platelet
5	$PDLLA_{32}$ - $b$ - $PLLA_{66}$	0.48	4600	4700	1.18	14,000	8300	1.28	platelet
6	PDLLA <sub>34</sub> -b-PLLA <sub>111</sub>	0.31	4900	5300	1.24	20,800	9800	1.34	platelet
7	PDLLA <sub>33</sub> -b-PLLA <sub>147</sub>	0.22	4700	5200	1.27	25,700	13,400	1.20	platelet
8	$\mathbf{PDLLA_{18}}\text{-}b\text{-}\mathbf{PLLA_{20}}$	0.90	2500	3000	1.20	5400	4600	1.18	sphere and platelet
9	$PDLLA_{18}$ - $b$ - $PLLA_{38}$	0.47	2500	3800	1.24	8000	7600	1.23	platelet
10	PDLLA <sub>18</sub> -b-PLLA <sub>59</sub>	0.31	2500	4000	1.22	11,000	11,500	1.22	platelet
11	${\tt PDLLA_{17}\text{-}}b\text{-}{\tt PLLA_{68}}$	0.25	2400	2700	1.23	12,300	7800	1.25	precipitate
12	$\mathbf{PDLLA}_{71}\text{-}b\text{-}\mathbf{PLLA}_{42}$	1.69	10,200	5100	1.19	16,200	7000	1.23	sphere
13	PDLLA <sub>64</sub> -b-PLLA <sub>73</sub>	0.88	9200	5500	1.15	19,700	8300	1.28	platelet
14	PDLLA <sub>66</sub> -b-PLLA <sub>135</sub>	0.49	9500	5900	1.22	28,900	12,500	1.33	platelet
15 <sup>e</sup>	$\mathbf{PDLLA}_{34}\text{-}b\text{-}\mathbf{PLLA}_{74}$	0.46	4900	4200	1.19	15,500	6500	1.35	sphere
16 <sup>e</sup>	$PDLLA_{36}$ - $b$ - $PLLA_{71}$	0.51	5100	5600	1.24	15,400	12,600	1.41	platelet

<sup>a</sup>PDLLA, DBU, and toluene were used as stabilizer/macroinitiator block, catalyst, and solvent, respectively. Polymerization temperature was set as 20 °C, solids content was set as 10% w/w, and stirring rate was set as 300 rpm. <sup>b</sup>Subscript represents the DP for each block, which was calculated according to monomer conversion (>96%) based on <sup>1</sup>H NMR spectra. <sup>c</sup> $M_{\rm n,GPC}$  and  $M_{\rm pv}/M_{\rm n}$  were determined using GPC, wherein THF and poly(methyl methacrylate) (PMMA) were used as the eluent and standard, respectively. <sup>d</sup>Morphologies were measured using HCTEM and field-emission scanning electron microscopy (FESEM). <sup>e</sup>Solids content was set as 5% w/w in entry 15 and 20% w/w in entry 16, respectively.

a temperature of 20 °C and a stirring rate of 300 rpm. As shown in Figure S1, the matrix-assisted laser desorption/ionization-time-of-flight mass spectrometry (MALDI-TOF MS) confirmed that the PDLLA possessing a 1-tetradecanol residue and a hydroxyl chain end was successfully synthesized

via DBU-catalyzed ROP. The gel permeation chromatography (GPC) curves with unimodal peaks confirmed that PDLLA and PDLLA-b-PLLA with controlled MW and narrow MW distribution  $(M_{\rm w}/M_{\rm n})$  were successfully prepared (Figure 1a). The conversion of the L-LA monomer can be calculated by  $^1$ H

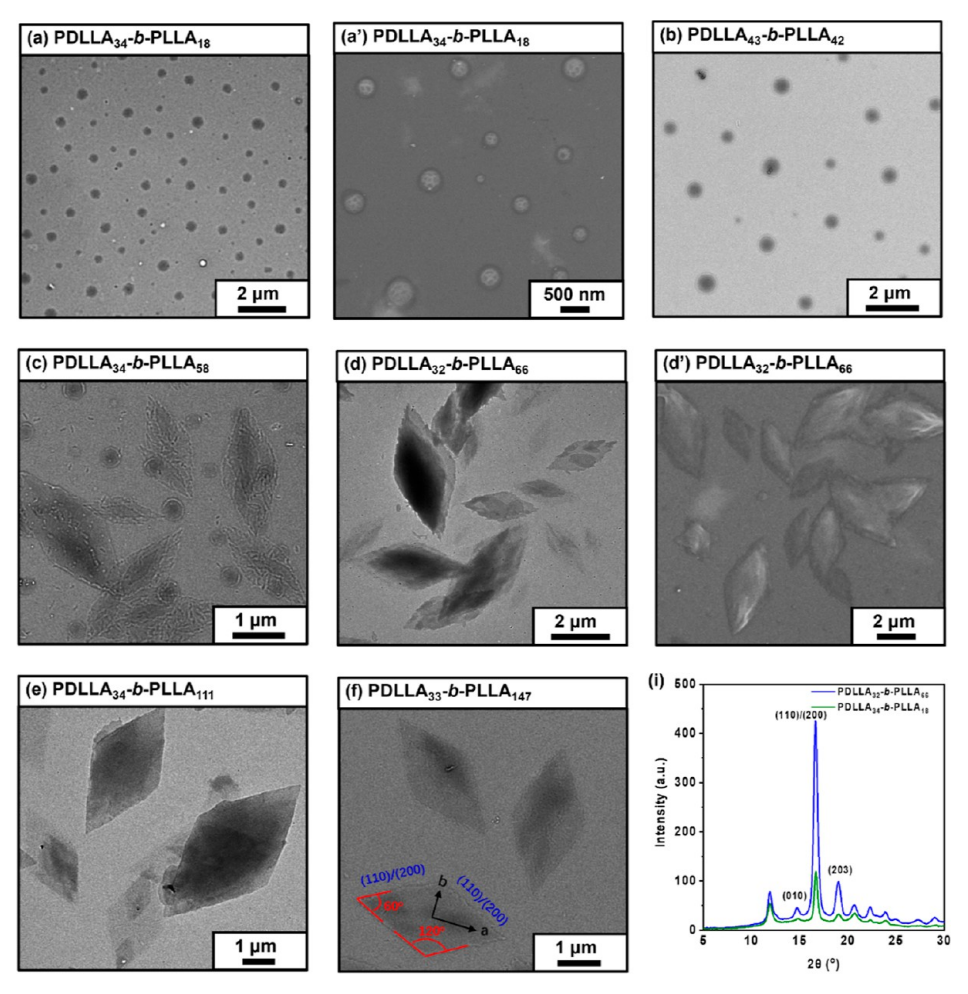


Figure 2. (a–f) HCTEM images of PDLLA-b-PLLA-based nano-objects generated from the ROPISA process with different DP<sub>PDLLA</sub>/DP<sub>PLLA</sub> in toluene. (a',d') FESEM images of the corresponding nano-objects. Nano-objects were diluted into 0.07–0.2% w/w dispersions. Samples on the copper grid were not stained. (i) Wide-angle X-ray scattering (WAXS) patterns of PDLLA<sub>34</sub>-b-PLLA<sub>18</sub>- and PDLLA<sub>32</sub>-b-PLLA<sub>66</sub>-based nano-objects

NMR spectra based on the variation of the resonance signals attributed to the methine proton  $(-CH(CH_3)COO-)$  at 4.89 ppm on the L-LA monomer and that at 5.35 ppm on the PLLA block (Figure 1b). Prolonging the polymerization time, the conversion of L-LA monomer was regularly increased, and the polymerization can be finished in 110 min (Figure 1c). The kinetics evolution of  $ln([M]_0/[M])$  versus time indicated that the polymerization process was realized with a fast first-order stage and followed by a relatively slow one. The kinetics evolution tendency was different to conventional reversible addition-fragmentation chain transfer (RAFT) PISA process<sup>26,31</sup> and the previous ROPISA process of the L-LA monomer, 41,42 in which the polymerization kinetics was featured with a slow first-order stage and followed by a relatively fast one. Alternatively, the polymerization kinetics in this work was rather similar to that for a typical solution polymerization of lactones<sup>49,50</sup> and a previous work on ROPISA of  $\varepsilon$ -CL and  $\delta$ -VL monomers. <sup>48</sup> The possible reason can be attributed to the balance between the polymerization rate of the L-LA monomer and the crystallization rate of the core-forming PLLA block, which might be affected by parameters (such as solvent, temperature, catalyst, etc.) employed in the PISA process. 41,42 In our case, the DBU catalyst might promote a fast polymerization rate, and the crystallization rate or self-assembly process was relatively

delayed even after the complete conversion of the monomer. Thus, the L-LA monomer might be dominantly polymerized in a relatively homogeneous stage without or with weak aggregation of copolymers, which still obeyed the kinetic behavior of a conventional solution polymerization process rather than a typical PISA process. The number-average molecular weight ( $M_{\rm n,GPC}$ ) of PDLLA-b-PLLA was regularly increased while maintaining narrow  $M_{\rm w}/M_{\rm n}$  (Figure 1d). However, the  $M_{\rm n,GPC}$  had an obvious derivation from  $M_{\rm n,theo}$  due to the relatively poor solubility of PDLLA-b-PLLA in THF elution. S1-53 Alternatively, in the following section, the  $M_{\rm n,NMR}$  calculated from  $^{1}$ H NMR spectra was adopted for all samples, and the derived DP was labeled as the subscript.

Morphological Evolution of PDLLA- $\bar{b}$ -PLLA-Based Nano-Objects in the ROPISA Process. The morphologies of the resulting nano-objects from the ROPISA process can be affected by multiple parameters. Herein, fixing the temperature at 20 °C and stirring rate at 300 rpm, the ROPISA process was dominantly investigated by varying  $\mathrm{DP_{PDLLA}}$  of the stabilizer/macroinitiator,  $\mathrm{DP_{PDLLA}}/\mathrm{DP_{PLLA}}$ , solvents, and solids content. As described in the above section, the crystallization rate or self-assembly process might be slower than the polymerization process. For consistency, the ROPISA process was continued for another 4.0 h with stirring at 300 rpm after the complete polymerization, and the sampling for high contrast trans-

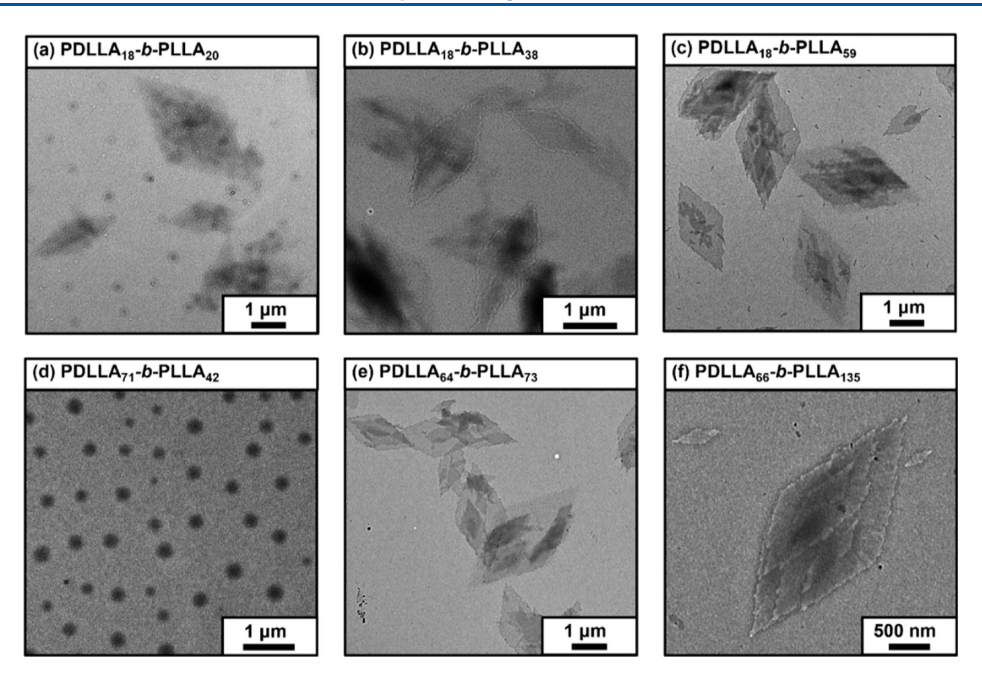


Figure 3. (a-f) HCTEM images of PDLLA-b-PLLA-based nano-objects generated from the ROPISA process with different  $DP_{PDLLA}/DP_{PLLA}$  in toluene. Nano-objects were diluted into 0.07-0.2% w/w dispersions. Samples on copper grid were not stained.

mission electron microscope (HCTEM) measurement was followed. The detailed results are summarized in Tables 1 and S1.

First, fixing the solids content at 10% w/w and DP<sub>PDLLA</sub> around 35, the morphologies of nano-objects derived from PDLLA-b-PLLA diblock copolymers were evaluated by HCTEM while varying the DP<sub>PDLLA</sub>/DP<sub>PLLA</sub> ratio. For the DP<sub>PDLLA</sub>/DP<sub>PLLA</sub> of 3.50, the PDLLA<sub>35</sub>-b-PLLA<sub>10</sub> block copolymer was formed, and no regular self-assembled structure could be discerned (entry 1 in Table 1). The reason can be attributed to shorter core-forming blocks and weaker aggregation ability of the block copolymers. As shown in Figure 2a (entry 2 in Table 1), PDLLA<sub>34</sub>-b-PLLA<sub>18</sub> was generated, and pure spheres were observed when the DP<sub>PDLLA</sub>/ DP<sub>PLLA</sub> was decreased to 1.89. When the DP<sub>PDLLA</sub>/DP<sub>PLLA</sub> was decreased to 1.02, the PDLLA<sub>43</sub>-b-PLLA<sub>42</sub> diblock copolymer was formed, and spheres were also collected from Figure 2b (entry 3 in Table 1). When the DP<sub>PDLLA</sub>/DP<sub>PLLA</sub> was decreased to 0.58, the PDLLA<sub>34</sub>-b-PLLA<sub>58</sub> diblock copolymer was generated, and a mixture of spheres and diamond-shaped platelets could be discriminated from Figure 2c (entry 4 in Table 1). When DP<sub>PDLLA</sub>/DP<sub>PLLA</sub> was further decreased from 0.48 to 0.31 and 0.22, PDLLA<sub>32</sub>-b-PLLA<sub>66</sub>, PDLLA<sub>34</sub>-b-PLLA<sub>111</sub>, and PDLLA<sub>33</sub>-b-PLLA<sub>147</sub> diblock copolymers comprising pure diamond-shaped platelets were synthesized, respectively (Figure 2d-f, entries 5-7 in Table 1). The FESEM images of the nano-objects based on PDLLA<sub>34</sub>-b-PLLA<sub>18</sub> and PDLLA<sub>33</sub>-b-PLLA<sub>66</sub> provided additional confirmation on their respective spheres and diamond-shaped platelets, aligning consistently with the images from HCTEM measurement (Figure 2a',d'). It should be noticed that, in most cases, the platelet nano-objects were composed of multiple layered crystalline structures. The reason might come from the overlapping of the generated platelets during either the self-assembly process or the sampling for the TEM measurement.

The WAXS measurement was also carried out on spherical and diamond-shaped nano-objects derived from PDLLA<sub>34</sub>-b-

PLLA<sub>18</sub> and PDLLA<sub>32</sub>-b-PLLA<sub>66</sub> (Figure 2i). The WAXS patterns illustrated that the crystalline PLLA exhibited peaks at distinct diffraction angles compared to amorphous PDLLA. Specifically, the most prominent peak at 16.6° corresponded to the diffraction of (110)/(200) planes, while the peak at 19.8° was attributed to the (203) plane. The micrometer-sized diamond-shaped nano-objects observed by HCTEM images precisely matched the crystal planes with (110)/(200) examined through WAXS, featuring the aspect ratio of the direction (b to a) ca. 0.58 (Figure 2f). Simultaneously, the angles of adjacent edges were measured as 60 and 120°, respectively. The diamond-shaped nano-objects conferred an advantageous low-curvature structure, which served to minimize the surface energy, akin to the self-assembled single crystals observed in traditional PLLA homopolymer. 54 Uniquely, the growth of single crystal remained unaffected by the PDLLA block. Additionally, the WAXS data offered semiquantitative insights into the degree of crystallinity across the samples. According to the literature, 55 defining the crystallinity of PLLA homopolymer as 1.00, the relative crystallinity of PLLA in nano-objects of PDLLA<sub>34</sub>-b-PLLA<sub>18</sub> and PDLLA<sub>33</sub>-b-PLLA<sub>66</sub> can be derived as 0.41 to 0.79, respectively. The results indicated that the spherical nanoobjects arose from the relatively lower crystallinity of coreforming PLLA, whereas the PLLA was featured with a higher crystallinity in the diamond-shaped nano-objects. In other words, the crystallinity of core-forming PLLA has a close relationship with the self-assembled morphologies.

Alternatively, decreasing the targeted  $\mathrm{DP}_{\mathrm{PDLLA}}$  as 17, the PDLLA $_{18}$ -b-PLLA $_{20}$  diblock copolymer was generated at the  $\mathrm{DP}_{\mathrm{PDLLA}}/\mathrm{DP}_{\mathrm{PLLA}}$  of 0.90. In this case, the spheres were dominantly formed with minor coexisting diamond-shaped platelets (Figure 3a, entry 8 in Table 1). When the  $\mathrm{DP}_{\mathrm{PDLLA}}/\mathrm{DP}_{\mathrm{PLLA}}$  was decreased from 0.47 to 0.31, the PDLLA $_{18}$ -b-PLLA $_{38}$  and PDLLA $_{18}$ -b-PLLA $_{59}$  diblock copolymers comprising diamond-shaped platelets were generated, respectively (Figure 3b,c, entries 9–10 in Table 1). When  $\mathrm{DP}_{\mathrm{PDLLA}}/\mathrm{DP}_{\mathrm{PLLA}}$  of 0.25 was further attempted, the PDLLA $_{17}$ -b-PLLA $_{68}$  diblock

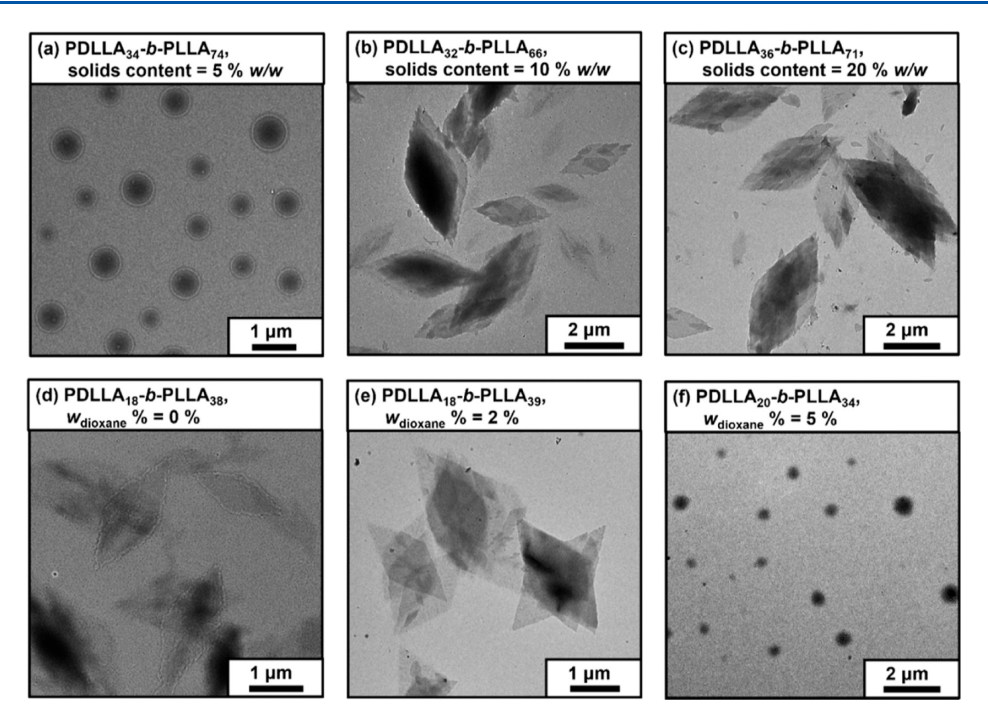


Figure 4. (a–c) HCTEM images of PDLLA-b-PLLA-based nano-objects (maintaining DP<sub>PDLLA</sub>/DP<sub>PLLA</sub> around 0.50) obtained by varying solids content in toluene. (d–f) HCTEM images of PDLLA-b-PLLA-based nano-objects (maintaining DP<sub>PDLLA</sub>/DP<sub>PLLA</sub> around 0.50) obtained with solids content of 10% w/w by varying solvents. Nano-objects were diluted into 0.07–0.2% w/w dispersions in the corresponding solvents for the ROPISA process. The sample on the copper grid was not stained.

copolymer were generated, and however, the precipitate was gradually observed (entry 11 in Table 1). Furthermore, designing the targeted DP<sub>PDLLA</sub> as 70, the resulting PDLLA<sub>71</sub>-b-PLLA<sub>42</sub> diblock copolymer with an DP<sub>PDLLA</sub>/ DP<sub>PLLA</sub> of 1.69 led to the formation of pure spheres (Figure 3d, entry 12 in Table 1). Similarly, when the DP<sub>PDLLA</sub>/DP<sub>PLLA</sub> was decreased from 0.88 to 0.49, PDLLA $_{64}$ -b-PLLA $_{73}$  and PDLLA<sub>66</sub>-b-PLLA<sub>135</sub> diblock copolymers were synthesized, respectively, and the diamond-shaped platelets were observed in both systems (Figure 3e,f, entries 13–14 in Table 1). Unlike the formation of precipitate in the case for PDLLA<sub>17</sub>-b-PLLA<sub>68</sub>, the longer PDLLA<sub>66</sub> efficiently increased the stability of PDLLA<sub>66</sub>-b-PLLA<sub>135</sub>-based nano-objects. Thus, it can be found that the morphological window can be efficiently comodulated by both  $DP_{PDLLA}$  of the PDLLA stabilizer and the  $DP_{PDLLA}$  $\mathrm{DP}_{\mathrm{PLLA}}$  ratio.

Second, the morphologies of nano-objects based on PDLLAb-PLLA diblock copolymers were evaluated by fixing the DP<sub>PDLLA</sub>/DP<sub>PLLA</sub> around 0.50 and DP<sub>PDLLA</sub> around 35 while varying the solids content. As shown in Figure 4a (entry 15 in Table 1), the PDLLA<sub>34</sub>-b-PLLA<sub>74</sub> diblock copolymer was generated at a solid content of 5% w/w, and only spheres were formed. When solids content was increased to 10% w/w and 20% w/w, PDLLA<sub>32</sub>-b-PLLA<sub>66</sub> and PDLLA<sub>36</sub>-b-PLLA<sub>71</sub> diblock copolymers were synthesized, respectively, and diamondshaped platelets were captured (Figure 4b,c, entries 5 and 16 in Table 1). In the case with lower solids content, lower-order spheres were favored, which might be attributed to the reduced collision and fusion of nano-objects. Alternatively, in the case with higher solids content, the relatively higher concentration greatly accelerated the collision and fusion of nano-objects, which facilitated the arrangement and crystallization of the PDLLA-b-PLLA copolymer, and the diamond-shaped platelets were generated. Thus, the solids content also has a significant effect on the morphological evolution of nano-objects.

Third, the effect of solvents on the ROPISA process was also studied. Maintaining the DP<sub>PDLLA</sub>/DP<sub>PLLA</sub> around 0.50, DP<sub>PDLLA</sub> around 35, and the solids content of 10% w/w, a good solvent of dioxane was introduced into the ROPISA system, and the effect was evaluated. When  $w_{\rm dioxane}$  % in toluene/dioxane cosolvent was set as 0%, the resulting PDLLA<sub>18</sub>-b-PLLA<sub>38</sub> diblock copolymer formed the diamondshaped platelets (Figure 4d, entry 1 in Table S1). When  $w_{\text{dioxane}}$ % was increased to 2%, the obtained PDLLA<sub>18</sub>-b-PLLA<sub>39</sub> diblock copolymer still contributed to the diamond-shaped platelets (Figure 4e, entry 2 in Table S1). Increasing the  $w_{\text{dioxane}}$  to 5%, however, the resulting PDLLA<sub>20</sub>-b-PLLA<sub>34</sub> diblock copolymer led to the formation of pure spheres, and the size was approximately 400 nm (Figure 4f, entry 3 in Table S1). Furthermore, when  $w_{\text{dioxane}}$  % was designed as 10%, the PDLLA<sub>18</sub>-b-PLLA<sub>36</sub> block copolymer was formed, and no regular self-assembled structure can be discriminated (entry 4 in Table S1). For a typical amorphous block copolymer, the solvophobic interactions between solvent and core-forming block are the driving force.<sup>56</sup> However, in a self-assembled system containing crystallizable core-forming blocks, the determinants impacting the assembly morphology are notably intricate and multifaceted. <sup>57,58</sup> The solubility and crystallinity should synergistically affect the self-assembly process. Thus, the variation of the solvent also has an obvious effect on the morphological evolution.

By summarizing the above results, it can be found that the diamond-shaped platelets can be captured at relatively higher  $\mathrm{DP}_{\mathrm{PLLA}}$ , higher solids content, and poorer solvents. On the contrary, only the spheres can be collected. Additionally, it should be noticed that all-polylactones nano-objects prepared by the PISA process were not as well-defined in shape or as

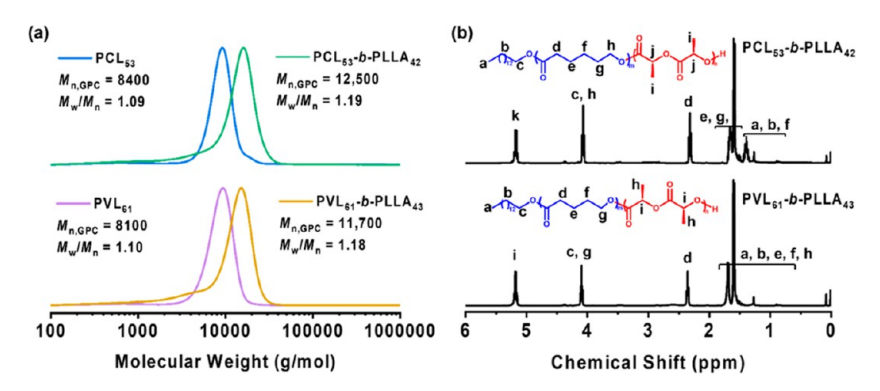


Figure 5. (a) GPC curves for the stabilizer/macroinitiator and the corresponding diblock copolymers in the ROPISA process (THF was used as eluent). (b) <sup>1</sup>H NMR spectra for PCL<sub>53</sub>-b-PLLA<sub>42</sub> and PVL<sub>61</sub>-b-PLLA<sub>43</sub> diblock copolymers (in CDCl<sub>3</sub>).

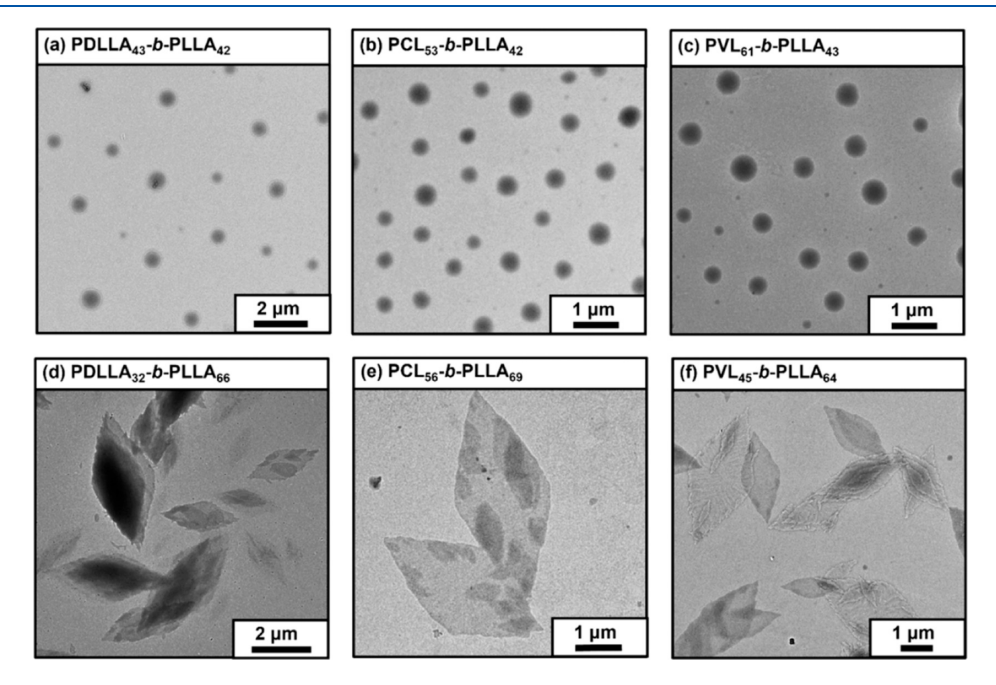


Figure 6. (a-f) HCTEM images of PDLLA-b-PLLA, PCL-b-PLLA, and PVL-b-PLLA-based nano-objects generated from the ROPISA process in toluene. Nano-objects were diluted into 0.07–0.2% w/w dispersions. Samples on the copper grid were not stained.

uniform in size as those produced by the traditional self-assembly technique. We have failed to modulate the shape and size by adjusting several experimental parameters. The reason can be attributed to the limitations of the ROPISA process itself, in which the shape and size might be significantly affected by both the polymerization behavior of the L-LA monomer and the crystallization behavior of the crystallizable core-forming PLLA block. Any fluctuation in the polymerization process might affect the crystallization behavior as well as the morphological evolution of the nano-objects. Comparatively, the parameters of the ROPISA process were more complicated than those for the traditional self-assembly process.

Scope of the Stabilizer/Macroinitiator Block for the ROPISA Process. In order to demonstrate wide applicability of the ROPISA process, PCL and PVL were also introduced as the stabilizer/macroinitiator blocks. Similar to the aforementioned PDLLA-*b*-PLLA diblock copolymer synthesized in the ROPISA process, we also set the temperature at 20 °C, the stirring rate at 300 rpm, the solid content at 10% w/w, and employed toluene as the solvent. Differently, methanesulfonic acid (MSA) and diphenylphosphate (DPP) were used as

organocatalysts for  $\varepsilon$ -CL and  $\delta$ -VL monomers at the first polymerization stage, respectively. The GPC results showed that the PCL-OH and PVL-OH stabilizer/macroinitiator blocks were first and successfully synthesized. After the chain extension, the GPC results clearly showed that the PCL-b-PLLA and PVL-b-PLLA diblock copolymers were formed (Figure 5a). However, due to the possible side reaction, such as the transesterification, 41 a trace amount of homopolymer with low MW was generated, and the GPC curves were exhibited with a tail. The characteristic resonance signals of the stabilizer/macroinitiator and the corresponding diblock copolymers attributed to the related protons were also observed from the <sup>1</sup>H NMR spectra (Figures S2-S3 and Figure 5b). The GPC and <sup>1</sup>H NMR confirmed that the PCL-b-PLLA- and PVL-b-PLLA-based ROPISA processes can also be realized in a controlled manner.

The PDLLA-b-PLLA, PCL-b-PLLA, or PVL-b-PLLA diblock copolymer with close  $\mathrm{DP}_{\mathrm{PDLLA}}/\mathrm{DP}_{\mathrm{PLLA}}$ ,  $\mathrm{DP}_{\mathrm{PCL}}/\mathrm{DP}_{\mathrm{PLLA}}$ ,  $\mathrm{DP}_{\mathrm{PVL}}/\mathrm{DP}_{\mathrm{PLLA}}$ , and MWs were designed and used as comparisons, and the detailed results were summarized in Table S2. For the  $\mathrm{DP}_{\mathrm{PDLLA}}/\mathrm{DP}_{\mathrm{PLLA}}$  of 1.02, the resulting PDLLA<sub>43</sub>-b-PLLA<sub>42</sub> diblock copolymer was synthesized, and

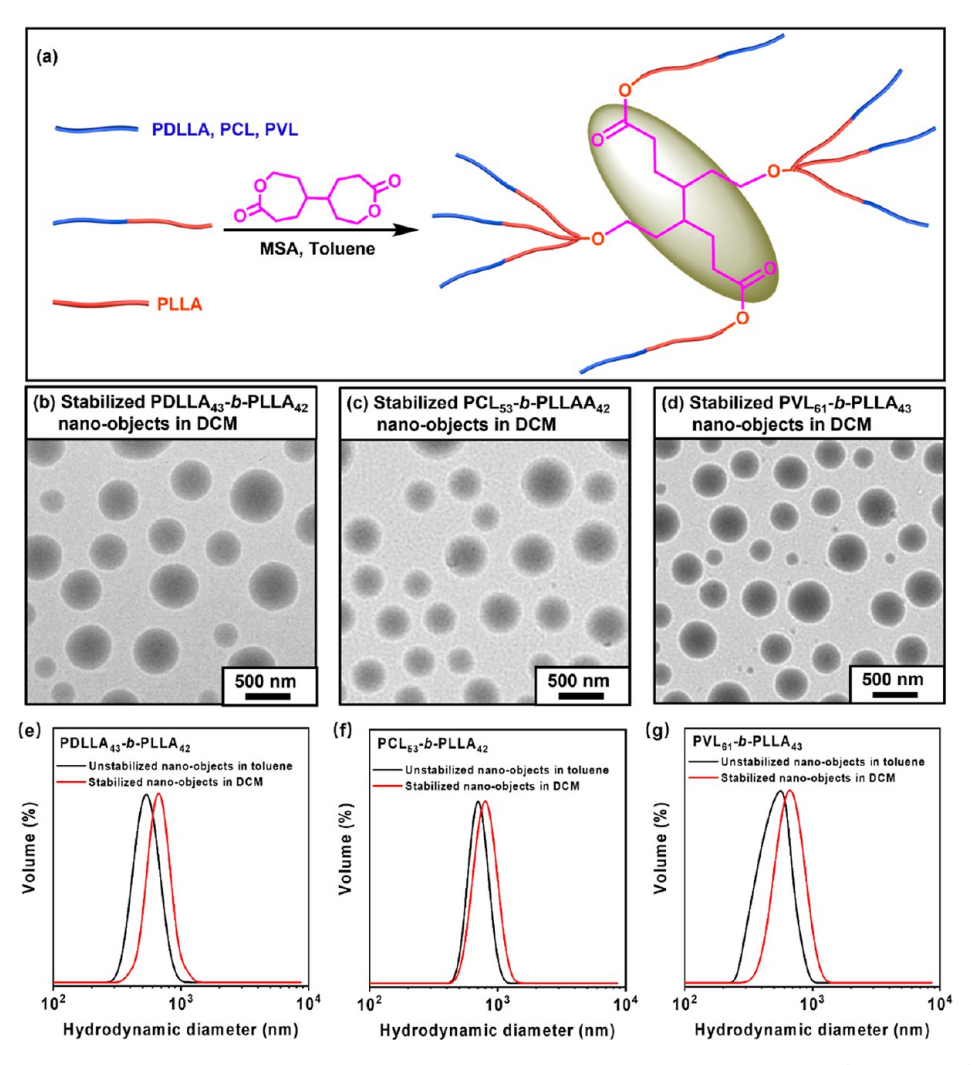


Figure 7. (a) Schematic of the stabilization of nano-objects in the final polymerization stage by BOD. PDLLA (PCL or PVL), L-LA, and toluene were stabilizer/macroinitiator block, monomer, and solvent, respectively. (b-d) HCTEM images of the stabilized nano-objects in dichloromethane (DCM). Samples were diluted into 0.1–0.2% w/w dispersions in DCM, and samples on copper grid were not stained. (e-g) dynamic light scattering (DLS) results of the stabilized and unstabilized nano-objects. Samples were diluted into 0.2–0.4% w/w dispersions.

the spheres were formed (Figure 6a, entry 1 in Table S2). The PDLLA<sub>32</sub>-b-PLLA<sub>66</sub> diblock copolymer was synthesized by decreasing DP<sub>PDLLA</sub>/DP<sub>PLLA</sub> as 0.48, leading to the formation of nano-objects with diamond-shaped platelets (Figure 6d, entry 2 in Table S2). Similarly, for the DP<sub>PCL</sub>/DP<sub>PLLA</sub> of 1.26 and 0.81, it was found that the PCL<sub>53</sub>-b-PLLA<sub>42</sub> and PCL<sub>56</sub>-b-PLLA<sub>69</sub> block copolymers also tended to form spheres and diamond-shaped platelets, respectively (Figure 6b,e, entries 3-4 in Table S2). In addition, for the DP<sub>PVL</sub>/DP<sub>PLLA</sub> of 1.42 and 0.70, the similar formulation led to the formation of PVL<sub>61</sub>-b-PLLA<sub>43</sub> and PVL<sub>45</sub>-b-PLLA<sub>64</sub> diblock copolymers, and the spheres and diamond-shaped platelets could be observed, respectively (Figure 6c,f, entries 5-6 in Table S2). Obviously, employing different lactone monomers, it was feasible to generate nano-objects composed of all-polylactones by the ROPISA process.

Stabilization of the Nano-Objects Formed in the ROPISA Process. Given in a detailed application, the nano-objects should be stabilized to maintain the self-assembled morphologies. Herein, the ROPISA process has a living and controlled character, and the monomer can be completely converted in a defined polymerization time. Thus, the cross-linking of the PLLA core-forming block can be *in situ* realized

by adding a cross-linker of 4,4'-bioxepanyl-7,7'-dione (BOD) after the complete consumption of the L-LA monomer (Figure 7a and Figure S4). That was, the nano-objects can be stabilized in the final polymerization stage.

As shown in Figure 7b, the stabilized nano-objects from PDLLA<sub>43</sub>-b-PLLA<sub>42</sub> diblock copolymer have a similar spherical morphology in DCM as the unstabilized one in toluene (entry 1 in Table S2). Maintaining the original spherical morphology in DCM confirmed the successful cross-linking of the coreforming block in nano-objects, as DCM was a good solvent for both PLLA and PDLLA blocks. Similarly, the nano-objects from PCL<sub>53</sub>-b-PLLA<sub>42</sub> (Figure 7c, entry 3 in Table S2) and PVL<sub>61</sub>-b-PLLA<sub>43</sub> (Figure 7d, entry 5 in Table S2) diblock copolymers can all be stabilized. The DLS results indicated that the sizes in DCM were slightly larger than those in toluene (Figure 7e-g). The reason can be attributed to the enhanced swelling of the stabilized nano-objects by the DCM solvent. These results obtained from HCTEM and DLS measurements affirmed that the spherical nano-objects formed in the ROPISA process had been selectively and efficiently stabilized.

However, for the diamond-like nano-objects, the same stabilization strategy was infeasible. This might be due to the higher crystallinity of the PLLA block in diamond-shaped

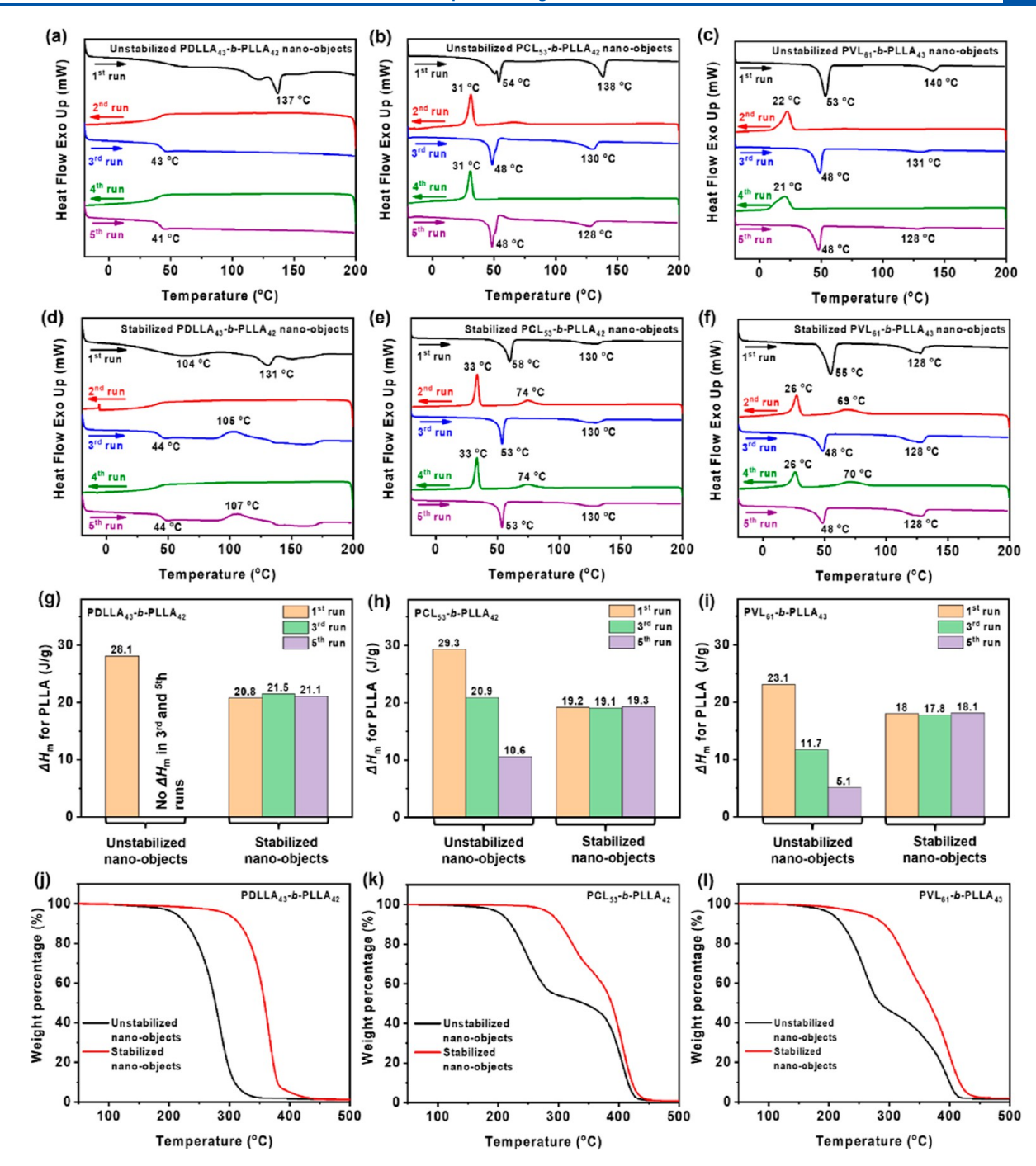


Figure 8. (a–f) DSC thermograms from consecutive runs for nano-objects synthesized from the ROPISA process. Samples were recovered from methanol, dried under a vacuum, and used for DSC measurement. Samples were heated or cooled between -20 and 200 °C in the first to fifth run. (g–i) Melting enthalpy value ( $\Delta H_{\rm m}$ ) of the PLLA block was determined by DSC from different runs for the stabilized and unstabilized nano-objects synthesized in ROPISA process. (j–l) TGA curves of the stabilized and unstabilized nano-objects synthesized in the ROPISA process.

nano-objects, which led to a more orderly arrangement and prevented the cross-linking reaction from the active hydroxyl groups at chain ends. Alternatively, in the case of spherical nano-objects, the PLLA block with relatively lower crystallinity facilitated the cross-linking reaction, and thus, the spherical nano-objects can be efficiently stabilized.

Thermal Behavior of All-Polylactones Nano-Objects from the ROPISA Process. As mentioned above, the PDLLA-*b*-PLLA, PCL-*b*-PLLA, and PVL-*b*-PLLA diblock copolymer-based all-polylactones nano-objects can be successfully prepared by the ROPISA process. For a practical

application, the thermal property was a key parameter for polylactone-based materials. Thus, the thermal analysis on all-polylactone nano-objects formed in the ROPISA process was further conducted by differential scanning calorimetry (DSC) and thermogravimetric analysis (TGA) measurements, respectively.

Before DSC analysis on nano-objects, PDLLA<sub>44</sub> and PLLA<sub>40</sub> homopolymers were first synthesized and subjected to a DSC measurement. As shown in Figure S5a, the DSC curve for PDLLA homopolymer showed a melting temperature  $(T_{\rm m})$  at 82 °C in the first heating run and a glass transition temperature

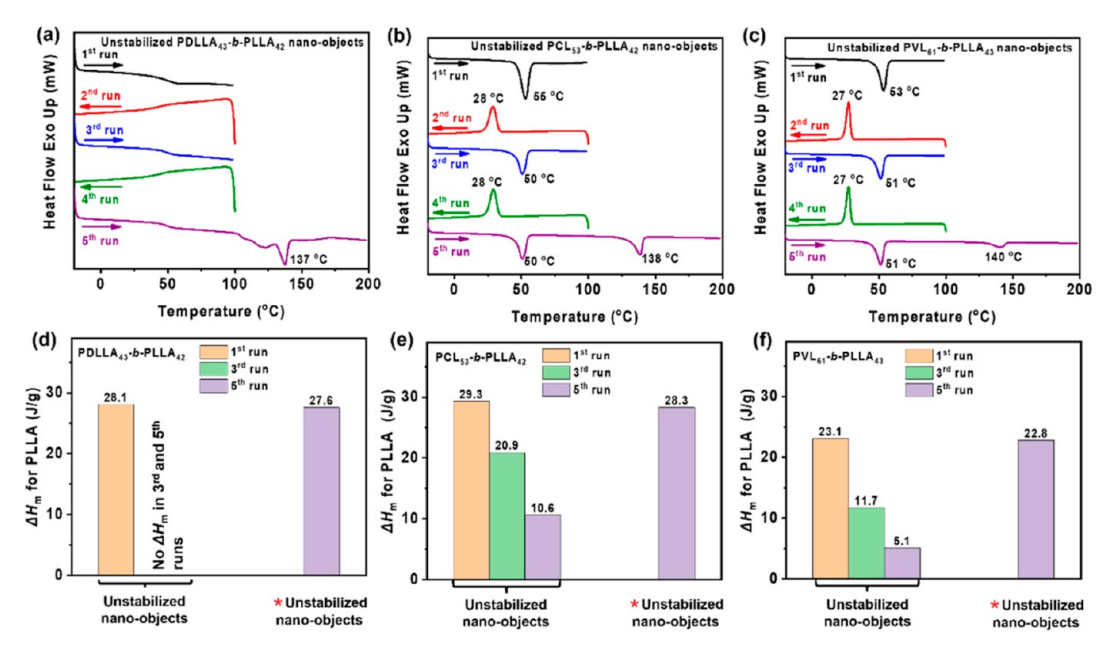


Figure 9. (a–c) DSC thermograms from consecutive runs for nano-objects synthesized from the ROPISA process (\*Samples were heated or cooled between -20 and 100 °C in the first to fourth run, while heated from -20 to 200 °C in the fifth heating run). (d–f) The  $\Delta H_{\rm m}$  of PLLA blocks was determined by DSC from different runs for the unstabilized nano-objects synthesized in the ROPISA process.

 $(T_{\rm g})$  around 35 °C in all heating/cooling run. In Figure S5b, the DSC curve for PLLA showed a  $T_{\rm m}$  at 141 °C in the first heating run and, however, no signal in the second cooling run. Alternatively, a weak crystallization temperature  $(T_{\rm c})$  at 95 °C and  $T_{\rm m}$  at 126 °C were observed in the third heating run. Continuously, no signal can be discriminated in the fourth cooling run, and a further weakened  $T_{\rm c}$  and  $T_{\rm m}$  were detected in the fifth heating run.

Using DSC curves for the PDLLA44 and PLLA40 homopolymers as references, the DSC curve for PDLLA43-b-PLLA<sub>42</sub> nano-objects was monitored and analyzed. It should be noted that both the stabilized and unstabilized nano-objects for DSC measurement were purified by dropping the ROPISA dispersions into methanol, which was simultaneously a poor solvent for PDLLA and PLA blocks. Thus, the spherical or diamond-shaped morphologies of nano-objects can be maintained. As shown in Figure 8a, the DSC curve for PDLLA<sub>43</sub>-b-PLLA<sub>42</sub> nano-objects showed a T<sub>m</sub> at 137 °C, which was attributed to PLLA block in the first heating run from -20 to 200 °C. Unexpectedly, no  $T_c$  can be observed from the DSC curve in the second cooling run from 200 to -20 °C, and only a  $T_{\rm g}$  at 43 °C can be detected. Continuously, in the third to fifth run, the  $T_{\rm m}$  and  $T_{\rm c}$  completely disappeared, while a  $T_g$  around 41 °C still remained.

Obviously, DSC results showed that the as-synthesized PDLLA block had a low crystallinity, which was destroyed and diminished after the first heating run, and only the amorphous PDLLA was reserved. Meanwhile, the as-synthesized PLLA block had a relatively high crystallinity, which was gradually weakened after the third and fifth heating runs. The reason for the disappearance of  $T_{\rm c}$  or  $T_{\rm m}$  on PDLLA or PLLA blocks was further probed by GPC measurements. GPC results before and after DSC measurement showed that the PDLLA<sub>43</sub> and PLLA<sub>40</sub> homopolymers, as well as the PDLLA<sub>43</sub>-b-PLLA<sub>42</sub> diblock copolymer, were subject to thermal degradation during the DSC measurement (Figure S6). The degraded fragments with low MW significantly weakened the crystallinity of PDLLA or PLLA blocks, which should be attributed to the

disappearance of  $T_{\rm c}$  or  $T_{\rm m}$  in DSC curves. Alternatively, in Figure 8d, when the PLLA block in the core region was cross-linked and the nano-objects were stabilized, the  $T_{\rm c}$  around 105 °C and  $T_{\rm m}$  around 131 °C can always be detected in the third and fifth heating runs in DSC curves. That was, the stabilization can greatly enhance the thermal stability of the PLLA block as well as the nano-objects.

During DSC cycles, the melting entropy ( $\Delta H_{\rm m}$ ) around 130 °C for PLLA blocks was summarized in Table S3. As shown in Figure 8g, it can be found that, for unstabilized nano-objects, the  $\Delta H_{\rm m}$  in the first heating run was 28.1 J/g, and no  $\Delta H_{\rm m}$  can be discriminated in the following third and fifth heating runs. However, for the stabilized nano-objects, the  $\Delta H_{\rm m}$  in the first heating run was 20.8 J/g, which can be well kept in the third (21.5 J/g) and fifth heating runs (21.1 J/g). The comparison on  $\Delta H_{\rm m}$  further confirmed that the thermal stability of the stabilized nano-objects can be greatly improved. Furthermore, the stabilized and unstabilized nano-objects were also subjected to a TGA measurement. As shown in Figure 8j, the thermal decomposition curve of unstabilized PDLLA<sub>43</sub>-b-PLLLA<sub>42</sub> nano-objects started at around 200 °C and ended at around 310 °C. Prominently, the decomposition temperature of the stabilized PDLLA<sub>43</sub>-b-PLLLA<sub>42</sub> nano-objects started at approximately 300 °C and ended at 400 °C. Obviously, the thermal stability of the stabilized PDLLA43-b-PLLLA42 nanoobjects has been enhanced by approximately 100 °C.

For stabilized or unstabilized  $PCL_{53}$ -b-PLLA<sub>42</sub> and  $PVL_{61}$ -b-PLLA<sub>43</sub> nano-objects, the evolution of  $T_c$  or  $T_m$  at around 130 °C for the PLLA block in DSC curves has a similar tendency as those from PDLLA<sub>43</sub>-b-PLLA<sub>42</sub> nano-objects. Differently, from the first to fifth heating run, the  $T_c$  and  $T_m$  for PCL block were detected at 31 and 48 °C (Figure 8b,e), and the  $T_c$  and  $T_m$  for PVL block were detected at 22 and 48 °C (Figure 8c,f), respectively. Obviously, the crystallization and melting processes of PCL, PVL, and PLLA were independent (Figure S5c,d). After DSC measurement, GPC curves for PCL, PVL, PCL-b-PLLA, and PVL-b-PLLA confirmed that there was no degradation on PCL and PVL blocks (Figure S7). However,

the PLLA block was still subjected to serious degradation. The  $\Delta H_{\rm m}$  of PLLA blocks for stabilized or unstabilized PCL<sub>53</sub>-b-PLLA<sub>42</sub> and PVL<sub>61</sub>-b-PLLA<sub>43</sub> nano-objects are summarized in Table S3. Again, in the third to fifth heating run, the  $\Delta H_{\rm m}$  gradually dropped for unstabilized nano-objects, while  $\Delta H_{\rm m}$  almost remained constant for stabilized nano-objects Figure 8h,i. From the TGA curves, it can be discriminated that the thermal stability of PLLA blocks in stabilized PCL<sub>53</sub>-b-PLLA<sub>42</sub> and PVL<sub>61</sub>-b-PLLA<sub>43</sub> nano-objects was also enhanced (Figure 8k,l).

DSC analysis on unstabilized PDLLA<sub>43</sub>-b-PLLA<sub>42</sub>, PCL<sub>53</sub>-b-PLLA<sub>42</sub>, and PVL<sub>61</sub>-b-PLLA<sub>43</sub> nano-objects was further performed by an alternative program as follows. The sample was heated or cooled between -20 and 100 °C in the first to fourth run, while heated from -20 to 200 °C in the fifth heating run. Interestingly, it was found that the  $T_{\rm m}$  peak of PLLA can be well remained in the fifth heating run at around 138 °C (Figure 9a-c). As shown in Figure 9d-f, the  $\Delta H_{\rm m}$ values for PLLA blocks in the fifth heating run remained similar to these values in the first heating run in Figure 8g-i. That was, under relatively low temperature (below 100 °C), the crystallization of the PLLA block was unaffected and kept, while PDLLA, PCL, and PVL blocks can subject to a typical melting and crystallization process. The thermal transition of the PDLLA, PCL, and PVL stabilizers and PLLA core-forming block was independent. With this character, all-polylactones nano-objects can be sufficiently blended with the matrix (such as PDLLA, PCL, or PVL) below 100 °C, while the encapsulated PLLA can preserve its morphologies and contribute intrinsic functions to the formed materials.

## CONCLUSIONS

In summary, all-polylactones nano-objects with crystalline PLLA as the core-forming block and amorphous PDLLA as the stabilizer/macroinitiator block were successfully generated by the ROPISA process in a one-pot manner. The ROPISA process was featured with high solids content up to 20% w/w. The factors, including the DP<sub>PDLLA</sub>, DP<sub>PLLA</sub>, solids content, and solvents, demonstrated significant influence on the formation of morphologies of spheres or diamond-shaped platelets. The ROPISA process was demonstrated with wide applicability for the all-polylactones system by successful preparation of nanoobjects with PCL or PVL as the stabilizer block, and PLLA as the core-forming block. Based on the living and controlled character of the ROPISA process, the formed nano-objects could be efficiently stabilized by in situ cross-linking of the living species using a difunctional BOD agent. The thermal analysis showed that the stabilization can significantly enhance the thermal stability of nano-objects. Due to the relatively high  $T_{\rm m}$  of PLLA in the core region and low  $T_{\rm m}$  or  $T_{\rm g}$  of PDLLA, PCL, or PVL in the shell region, the original morphologies and intrinsic function of the nano-objects can be well maintained in a given composite system. Thus, the proof-of-concept experiments in this work have demonstrated that the ROPISA process was a promising method for all-polylactones nanoobjects.

#### ASSOCIATED CONTENT

#### **Solution** Supporting Information

The Supporting Information is available free of charge at https://pubs.acs.org/doi/10.1021/acs.macromol.4c01334.

Experimental section; MALDI-TOF MS spectrum for PDLLA<sub>18</sub>; <sup>1</sup>H NMR spectra for PCL<sub>53</sub>, PVL<sub>61</sub>, and BOD; DSC thermograms for homopolymers before or after DSC; GPC curves for (co)polymers before or after DSC measurement; and data of the formulation, characterization, morphologies, and thermal properties of the stabilized and unstabilized nano-objects formed in the ROPISA process (PDF)

#### AUTHOR INFORMATION

#### **Corresponding Author**

Guowei Wang — State Key Laboratory of Molecular Engineering of Polymers, Department of Macromolecular Science, Fudan University, Shanghai 200433, China; orcid.org/0000-0003-2595-8269; Email: gwwang@fudan.edu.cn

#### **Authors**

Ding Shen – State Key Laboratory of Molecular Engineering of Polymers, Department of Macromolecular Science, Fudan University, Shanghai 200433, China

Boyang Shi — State Key Laboratory of Molecular Engineering of Polymers, Department of Macromolecular Science, Fudan University, Shanghai 200433, China

Peng Zhou — State Key Laboratory of Molecular Engineering of Polymers, Department of Macromolecular Science, Fudan University, Shanghai 200433, China

Di Li — State Key Laboratory of Molecular Engineering of Polymers, Department of Macromolecular Science, Fudan University, Shanghai 200433, China; orcid.org/0000-0001-9017-9582

Wenya Zhu — State Key Laboratory of Molecular Engineering of Polymers, Department of Macromolecular Science, Fudan University, Shanghai 200433, China

Complete contact information is available at: https://pubs.acs.org/10.1021/acs.macromol.4c01334

#### Notes

The authors declare no competing financial interest.

#### ■ ACKNOWLEDGMENTS

We thank financial support by the National Natural Science Foundation of China (22271058).

## REFERENCES

- (1) Hu, S. Y.; Zhao, J. P.; Zhang, G. Z.; Schlaad, H. Macromolecular Architectures through Organocatalysis. *Prog. Polym. Sci.* **2017**, *74*, 34–77.
- (2) Song, Q. L.; Hu, S. Y.; Zhao, J. P.; Zhang, G. Z. Organocatalytic Copolymerization of Mixed Type Monomers. *Chin. J. Polym. Sci.* **2017**, 35 (5), 581–601.
- (3) Yu, W.; Maynard, E.; Chiaradia, V.; Arno, M. C.; Dove, A. P. Aliphatic Polycarbonates from Cyclic Carbonate Monomers and Their Application as Biomaterials. *Chem. Rev.* **2021**, *121* (18), 10865–10907.
- (4) Thulasisingh, A.; Kumar, K.; Yamunadevi, B.; Poojitha, N.; SuhailMadharHanif, S.; Kannaiyan, S. Biodegradable Packaging Materials. *Polym. Bull.* **2022**, *79* (7), 4467–4496.
- (5) Jandas, P. J.; Mohanty, S.; Nayak, S. K. Sustainability, Compostability, and Specific Microbial Activity on Agricultural Mulch Films Prepared from Poly(lactic acid). *Ind. Eng. Chem. Res.* **2013**, 52 (50), 17714–17724.

- (6) Uhrich, K. E.; Cannizzaro, S. M.; Langer, R. S.; Shakesheff, K. M. Polymeric Systems for Controlled Drug Release. *Chem. Rev.* **1999**, *99* (11), 3181–3198.
- (7) Lee, A. L. Z.; Voo, Z. X.; Chin, W.; Ono, R. J.; Yang, C.; Gao, S. J.; Hedrick, J. L.; Yang, Y. Y. Injectable Coacervate Hydrogel for Delivery of Anticancer Drug-Loaded Nanoparticles in vivo. ACS Appl. Mater. Interfaces 2018, 10 (16), 13274–13282.
- (8) Cheng, R.; Wang, X. Y.; Chen, W.; Meng, F. H.; Deng, C.; Liu, H. Y.; Zhong, Z. Y. Biodegradable Poly( $\varepsilon$ -caprolactone)-g-poly(2-hydroxyethyl methacrylate) Graft Copolymer Micelles as Superior Nano-carriers for "Smart" Doxorubicin Release. *J. Mater. Chem.* **2012**, 22 (23), 11730–11738.
- (9) Chin, A. L.; Wang, X. Q.; Tong, R. Aliphatic Polyester-Based Materials for Enhanced Cancer Immunotherapy. *Macromol. Biosci.* **2021**, *21* (7), 2100087.
- (10) Wang, Z. L.; Xu, Y.; Wang, Y.; Ito, Y.; Zhang, P. B.; Chen, X. S. Enhanced in Vitro Mineralization and in Vivo Osteogenesis of Composite Scaffolds through Controlled Surface Grafting of L-Lactic Acid Oligomer on Nanohydroxyapatite. *Biomacromolecules* **2016**, *17* (3), 818–829.
- (11) Zhang, W. J.; Feng, C.; Yang, G. Z.; Li, G. L.; Ding, X.; Wang, S. Y.; Dou, Y. D.; Zhang, Z. Y.; Chang, J.; Wu, C. T.; Jiang, X. Q. 3D-printed Scaffolds with Synergistic Effect of Hollow-pipe Structure and Bioactive Ions for Vascularized Bone Regeneration. *Biomaterials* **2017**, 135, 85–95.
- (12) Lai, Y. X.; Li, Y.; Cao, H. J.; Long, J.; Wang, X. L.; Li, L.; Li, C. R.; Jia, Q. Y.; Teng, B.; Tang, T. T.; Peng, J.; Eglin, D.; Alini, M.; Grijpma, D. W.; Richards, G.; Qin, L. Osteogenic magnesium incorporated into PLGA/TCP porous scaffold by 3D printing for repairing challenging bone defect. *Biomaterials* **2019**, *197*, 207–219.
- (13) Mecking, S. Nature or Petrochemistry? Biologically Degradable Materials. *Angew. Chem., Int. Ed.* **2004**, 43 (9), 1078–1085.
- (14) Moya-Lopez, C.; Gonzalez-Fuentes, J.; Bravo, I.; Chapron, D.; Bourson, P.; Alonso-Moreno, C.; Hermida-Merino, D. Polylactide Perspectives in Biomedicine: From Novel Synthesis to the Application Performance. *Pharmaceutics* **2022**, *14* (8), 1673.
- (15) Fu, J.; Luan, B.; Yu, X.; Cong, Y.; Li, J.; Pan, C. Y.; Han, Y. C.; Yang, Y. M.; Li, B. Y. Self-assembly of Crystalline-coil Diblock Copolymer in Solvents with Varying Selectivity: From Spinodal-like Aggregates to Spheres, Cylinders, and Lamellae. *Macromolecules* **2004**, 37 (3), 976–986.
- (16) Petzetakis, N.; Dove, A. P.; O'Reilly, R. K. Cylindrical Micelles from the Living Crystallization-Driven Self-Assembly of Poly(lactide)-containing Block Copolymers. *Chem. Sci.* **2011**, 2 (5), 955–960.
- (17) Sun, L.; Pitto-Barry, A.; Kirby, N.; Schiller, T. L.; Sanchez, A. M.; Dyson, M. A.; Sloan, J.; Wilson, N. R.; O'Reilly, R. K.; Dove, A. P. Structural Reorganization of Cylindrical Nanoparticles Triggered by Polylactide Stereocomplexation. *Nat. Commun.* **2014**, *5*, 5746.
- (18) Pitto-Barry, A.; Kirby, N.; Dove, A. P.; O'Reilly, R. K. Expanding the scope of the crystallization-driven self-assembly of polylactide-containing polymers. *Polym. Chem.* **2014**, *5* (4), 1427–1436.
- (19) Inam, M.; Foster, J. C.; Gao, J. Y.; Hong, Y. X.; Du, J. Z.; Dove, A. P.; O'Reilly, R. K. Size and Shape Affects the Antimicrobial Activity of Quaternized Nanoparticles. *J. Polym. Sci., Part A: Polym. Chem.* **2019**, *57* (3), 255–259.
- (20) Inam, M.; Jones, J. R.; Perez-Madrigal, M. M.; Arno, M. C.; Dove, A. P.; O'Reilly, R. K. Controlling the Size of Two-Dimensional Polymer Platelets for Water-in-Water Emulsifiers. *ACS Cent. Sci.* **2018**, *4* (1), 63–70.
- (21) Arno, M. C.; Inam, M.; Weems, A. C.; Li, Z. H.; Binch, A. L. A.; Platt, C. I.; Richardson, S. M.; Hoyland, J. A.; Dove, A. P.; O'Reilly, R. K. Exploiting the Role of Nanoparticle Shape in Enhancing Hydrogel Adhesive and Mechanical Properties. *Nat. Commun.* **2020**, *11* (1), 1420.
- (22) He, X. M.; He, Y. X.; Hsiao, M. S.; Harniman, R. L.; Pearce, S.; Winnik, M. A.; Manners, I. Complex and Hierarchical 2D Assemblies via Crystallization-Driven Self-Assembly of Poly(L-lactide) Homopol-

- ymers with Charged Termini. J. Am. Chem. Soc. 2017, 139 (27), 9221-9228.
- (23) Li, Z.; Sun, L.; Zhang, Y. F.; Dove, A. P.; O'Reilly, R. K.; Chen, G. S. Shape Effect of Glyco-Nanoparticles on Macrophage Cellular Uptake and Immune Response. *ACS Macro Lett.* **2016**, *5* (9), 1059–1064.
- (24) Li, Z.; Zhang, Y. F.; Wu, L. B.; Yu, W.; Wilks, T. R.; Dove, A. P.; Ding, H. M.; O'Reilly, R. K.; Chen, G. S.; Jiang, M. Glyco-Platelets with Controlled Morphologies via Crystallization-Driven Self-Assembly and Their Shape-Dependent Interplay with Macrophages. *ACS Macro Lett.* **2019**, *8* (5), 596–602.
- (25) Nicolas, J.; Mura, S.; Brambilla, D.; Mackiewicz, N.; Couvreur, P. Design, Functionalization Strategies and Biomedical Applications of Targeted Biodegradable/Biocompatible Polymer-based Nanocarriers for Drug Delivery. *Chem. Soc. Rev.* **2013**, 42 (3), 1147–1235.
- (26) Canning, S. L.; Smith, G. N.; Armes, S. P. A Critical Appraisal of RAFT-Mediated Polymerization-Induced Self Assembly. *Macromolecules* **2016**, 49 (6), 1985–2001.
- (27) Wang, G.; Schmitt, M.; Wang, Z. Y.; Lee, B.; Pan, X. C.; Fu, L. Y.; Yan, J. J.; Li, S. P.; Xie, G. J.; Bockstaller, M. R.; Matyjaszewski, K. Polymerization-Induced Self-Assembly (PISA) Using ICAR ATRP at Low Catalyst Concentration. *Macromolecules* **2016**, *49* (22), 8605–8615
- (28) Wang, J.; Wu, Z. G.; Wang, G. W.; Matyjaszewski, K. In Situ Crosslinking of Nanoparticles in Polymerization-Induced Self-Assembly via ARGET ATRP of Glycidyl Methacrylate. *Macromol. Rapid Commun.* **2019**, 40 (2), 1800332.
- (29) Zhang, W. J.; Hong, C. Y.; Pan, C. Y. Polymerization-Induced Self-Assembly of Functionalized Block Copolymer Nanoparticles and Their Application in Drug Delivery. *Macromol. Rapid Commun.* **2019**, 40 (2), 1800279.
- (30) Wang, J.; Cao, M. Y.; Zhou, P.; Wang, G. W. Exploration of a Living Anionic Polymerization Mechanism into Polymerization-Induced Self-Assembly and Site-Specific Stabilization of the Formed Nano-Objects. *Macromolecules* **2020**, *53* (8), 3157–3165.
- (31) Derry, M. J.; Fielding, L. A.; Armes, S. P. Polymerization-Induced Self-Assembly of Block Copolymer Nanoparticles via RAFT Non-aqueous Dispersion Polymerization. *Prog. Polym. Sci.* **2016**, *52*, 1–18.
- (32) Shi, B. Y.; Wang, G. W. Application of Polymerization-Induced Self-Assembly (PISA) Technology. *Acta Polym. Sin.* **2022**, *53* (1), 15–29.
- (33) Niu, B.; Chen, Y.; Zhang, L.; Tan, J. B. Organic-inorganic Hybrid Nanomaterials Prepared via Polymerization-Induced Self-Assembly: Recent Developments and Future Opportunities. *Polym. Chem.* **2022**, *13* (18), 2554–2569.
- (34) Qiu, L.; Han, X. Y.; Xing, C. F.; Glebe, U. Polymerization-Induced Self-Assembly: An Emerging Tool for Generating Polymer-Based Biohybrid Nanostructures. *Small* **2023**, *19* (18), No. e2207457.
- (35) Boott, C. E.; Gwyther, J.; Harniman, R. L.; Hayward, D. W.; Manners, I. Scalable and Uniform 1D Nanoparticles by Synchronous Polymerization, Crystallization and Self-Assembly. *Nat. Chem.* **2017**, *9* (8), 785–792.
- (36) Oliver, A. M.; Gwyther, J.; Boott, C. E.; Davis, S.; Pearce, S.; Manners, I. Scalable Fiber-like Micelles and Block Co-micelles by Polymerization-Induced Crystallization-Driven Self-Assembly. *J. Am. Chem. Soc.* **2018**, *140* (51), 18104–18114.
- (37) Lohmeijer, B. G. G.; Pratt, R. C.; Leibfarth, F.; Logan, J. W.; Long, D. A.; Dove, A. P.; Nederberg, F.; Choi, J.; Wade, C.; Waymouth, R. M.; Hedrick, J. L. Guanidine and Amidine Organocatalysts for Ring-Opening Polymerization of Cyclic Esters. *Macromolecules* **2006**, 39 (25), 8574–8583.
- (38) Gazeau-Bureau, S.; Delcroix, D.; Martín-Vaca, B.; Bourissou, D.; Navarro, C.; Magnet, S. Organo-catalyzed ROP of  $\varepsilon$ -caprolactone: Methanesulfonic AcidCompetes with Trifluoromethanesulfonic Acid. *Macromolecules* **2008**, *41* (11), 3782–3784.
- (39) Makiguchi, K.; Satoh, T.; Kakuchi, T. Diphenyl Phosphate as an Efficient Cationic Organocatalyst for Controlled/Living Ring-

- Opening Polymerization of  $\delta$ -Valerolactone and  $\epsilon$ -Caprolactone. *Macromolecules* **2011**, 44 (7), 1999–2005.
- (40) Jiang, J.; Zhu, Y.; Du, J. Challenges and Perspective on Ring-Opening Polymerization-Induced Self-Assembly. *Acta Chim. Sin.* **2020**, 78 (8), 719–724.
- (41) Hurst, P. J.; Rakowski, A. M.; Patterson, J. P. Ring-Opening Polymerization-Induced Crystallization-Driven Self-Assembly of poly-<sub>L</sub>-lactide-*block*-polyethylene Glycol Block Copolymers (ROPI-CDSA). *Nat. Commun.* **2020**, *11* (1), 4690.
- (42) Hurst, P. J.; Graham, A. A.; Patterson, J. P. Gaining Structural Control by Modification of Polymerization Rate in Ring-Opening Polymerization-Induced Crystallization-Driven Self-Assembly. *ACS Polym. Au* 2022, 2 (6), 501–509.
- (43) Jiang, J. H.; Zhang, X. Y.; Fan, Z.; Du, J. Z. Ring-Opening Polymerization of N-Carboxyanhydride-Induced Self-Assembly for Fabricating Biodegradable Polymer Vesicles. *ACS Macro Lett.* **2019**, 8 (10), 1216–1221.
- (44) Grazon, C.; Salas-Ambrosio, P.; Ibarboure, E.; Buol, A.; Garanger, E.; Grinstaff, M. W.; Lecommandoux, S.; Bonduelle, C. Aqueous Ring-Opening Polymerization Induced Self-Assembly (ROPISA) of N-carboxyanhydrides. *Angew. Chem., Int. Ed.* **2020**, 59 (2), 622–626.
- (45) Grazon, C.; Salas-Ambrosio, P.; Antoine, S.; Ibarboure, E.; Sandre, O.; Clulow, A. J.; Boyd, B.; Grinstaff, M. W.; Lecommandoux, S.; Bonduelle, C. Aqueous ROPISA of  $\alpha$ -amino acid N-carboxyanhydrides: polypeptide block secondary structure controls nanoparticle shape anisotropy. *Polym. Chem.* **2021**, *12* (43), 6242–6251.
- (46) Shi, Q. Q.; Chen, Y. B.; Yang, J. J.; Yang, J. Ring-Opening Polymerization-Induced Self-Assembly (ROPISA) of Salicylic Acid o-Carboxyanhydride. *Chem. Commun.* **2021**, *57* (86), 11390–11393.
- (47) Ellis, C. E.; Garcia-Hernandez, J. D.; Manners, I. Scalable and Uniform Length-Tunable Biodegradable Block Copolymer Nanofibers with a Polycarbonate Core via Living Polymerization-Induced Crystallization-Driven Self-assembly. *J. Am. Chem. Soc.* **2022**, 144 (44), 20525–20538.
- (48) Shen, D.; Shi, B. Y.; Zhou, P.; Li, D.; Wang, G. W. Temperature-Dependent Ring-Opening Polymerization-Induced Self-Assembly Using Crystallizable Polylactones as Core-Forming Blocks. *Macromolecules* **2023**, *56* (13), 4814–4822.
- (49) Schneiderman, D. K.; Hillmyer, M. A. Aliphatic Polyester Block Polymer Design. *Macromolecules* **2016**, 49 (7), 2419–2428.
- (50) Bourissou, D.; Martin-Vaca, B.; Dumitrescu, A.; Graullier, M.; Lacombe, F. Controlled Cationic Polymerization of Lactide. *Macromolecules* **2005**, 38 (24), 9993–9998.
- (51) Wolf, F. K.; Hofmann, A. M.; Frey, H. Poly(isoglycerol methacrylate)-b-poly( $_{\rm D}$  or  $_{\rm L}$ -lactide) Copolymers: A Novel Hydrophilic Methacrylate as Building Block for Supramolecular Aggregates. *Macromolecules* **2010**, 43 (7), 3314–3324.
- (52) Razuvaeva, E. V.; Kulebyakina, A. I.; Streltsov, D. R.; Bakirov, A. V.; Kamyshinsky, R. A.; Kuznetsov, N. M.; Chvalun, S. N.; Shtykova, E. V. Effect of Composition and Molecular Structure of Poly(L-lactic acid)/Poly(ethylene oxide) Block Copolymers on Micellar Morphology in Aqueous Solution. *Langmuir* **2018**, 34 (50), 15470–15482.
- (53) Noack, S.; Schanzenbach, D.; Koetz, J.; Schlaad, H. Polylactide-Based Amphiphilic Block Copolymers: Crystallization-Induced Self-Assembly and Stereocomplexation. *Macromol. Rapid Commun.* **2019**, 40 (1), 1800639.
- (54) He, W. N.; Xu, J. T. Crystallization Assisted Self-Assembly of Semicrystalline Block Copolymers. *Prog. Polym. Sci.* **2012**, *37* (10), 1350–1400.
- (55) Sun, L.; Petzetakis, N.; Pitto-Barry, A.; Schiller, T. L.; Kirby, N.; Keddie, D. J.; Boyd, B. J.; O'Reilly, R. K.; Dove, A. P. Tuning the Size of Cylindrical Micelles from Poly(<sub>L</sub>-lactide)-b-poly(acrylic acid) Diblock Copolymers Based on Crystallization-Driven Self-Assembly. *Macromolecules* **2013**, *46* (22), 9074–9082.
- (56) Lu, Y. Q.; Lin, J. P.; Wang, L. Q.; Zhang, L. S.; Cai, C. H. Self-Assembly of Copolymer Micelles: Higher-Level Assembly for

- Constructing Hierarchical Structure. Chem. Rev. 2020, 120 (9), 4111-4140.
- (57) Zhulina, E. B.; Adam, M.; LaRue, I.; Sheiko, S. S.; Rubinstein, M. Diblock Copolymer Micelles in a Dilute Solution. *Macromolecules* **2005**, 38 (12), 5330–5351.
- (58) Shi, B. Y.; Shen, D.; Li, W.; Wang, G. W. Self-Assembly of Copolymers Containing Crystallizable Blocks: Strategies and Applications. *Macromol. Rapid Commun.* **2022**, 43 (14), 2200071.
- (59) Qu, Q. W.; Liu, G. Y.; Lv, X. Q.; Zhang, B. H.; An, Z. S. In Situ Cross-Linking of Vesicles in Polymerization-Induced Self Assembly. *ACS Macro Lett.* **2016**, *5* (3), 316–320.
- (60) Chen, M.; Li, J. W.; Zhang, W. J.; Hong, C. Y.; Pan, C. Y. pH-and Reductant-Responsive Polymeric Vesicles with Robust Membrane-Cross-Linked Structures: In Situ Cross-Linking in Polymerization-Induced Self-Assembly. *Macromolecules* **2019**, *52* (3), 1140–1149.